ELSEVIER

Chemical Engineering Journal 139 (2008) 416–425

Chemical Engineering Journal

www.elsevier.com/locate/cej

Role of phase behavior in micronization of lysozyme via a supercritical anti-solvent process

Shan-Chun Chang, Ming-Jer Lee, Ho-Mu Lin *

Department of Chemical Engineering, National Taiwan University of Science and Technology, 43 Keelung Road, Section 4, Taipei 106-07, Taiwan

Received 7 May 2007; received in revised form 16 November 2007; accepted 4 December 2007

Abstract

Ultra-fine particles of protein lysozyme were prepared with a supercritical anti-solvent (SAS) apparatus by using dimethyl sulfoxide (DMSO) as solvent and carbon dioxide as anti-solvent. The influences of various experimental factors on the morphology and the mean size of particulate products were investigated. As evidenced from the experimental results, phase behavior of the mixtures in precipitator during the particle formation stage played a crucial role in the SAS processes. Uniform networked nano-particles were obtained when the precipitations were conducted in the supercritical region of carbon dioxide + DMSO mixture. Several different types of morphologies were produced simultaneously as the precipitations were operated near the critical region. Spherical micron-scale clusters were formed in the superheated vapor region, while submicron-particles were aggregated as dense cake when lysozyme precipitated in the vapor–liquid coexistence region. The wide angle X-ray scattering (WAXS) patterns indicated that both the raw lysozyme and the processed particulate samples were amorphous. The differential scanning calorimeter (DSC) thermograms showed that the dehydration peak was disappeared after SAS treatment. Moreover, the networked primary particles could be disintegrated and dispersed well in water through ultrasonication, which were confirmed by analysis with dynamic laser scattering (DLS). A continuous stirred tank reactor (CSTR) model was used to calculate the dynamic composition variations of the mixtures in precipitator during the particle formation period.
© 2008 Published by Elsevier B.V.

Keywords: Supercritical anti-solvent; Micronization process; Lysozyme; Phase behavior

1. Introduction

In the past few decades, various micronization methods have been developed to produce ultra-fine particles for many applications. The traditional micronization methods, such as milling, grinding, sol–gel, and spray drying, have certain inherent limitations in particle formations for proteins and pharmaceutical compounds. For example, denaturation or degradation of particulate products may occur due to appreciable heat of friction being released during the processing, unacceptably high levels of residual solvents left in the particles, or the resultant products having broad particle size distribution (PSD) [1,2]. Supercritical fluid-assisted micronization processes are viable alternatives since these techniques are capable of overcoming the drawbacks of the conventional processes as mentioned above. These innovative methods include the rapid expansion of supercritical solutions (RESS) [3], the particles from gas-saturated solutions (PGSS) [4], the supercritical anti-solvent (SAS) [5], the supercritical-assisted atomization (SAA) [6], and the carbon dioxide-assisted nebulization with a bubble dryer® (CAN-BD) [7]. Among several others, Jung and Perrut [8], Vemavarapu et al. [9], and Reverchon and Adami [10] extensively surveyed the available articles and patents for the particle formations with the supercritical fluid technologies.

Recently, therapeutic proteins and peptides have received a great attention for the treatment of many diseases [11]. Fine particles with uniform size, ranging from 1 μm to 5 μm, are essential to the applications for pulmonary delivery and controlled release systems [12]. Proteins are often stored as dry powders to improve the long-term stability since the chemical and the physical degradations are facilitated by water contents in products [13]. Typically, the purposes of proteins micronization are to reduce necessary drug dose, to enhance bioavailability, or to build precise drug delivery systems.

* Corresponding author. Tel.: +886 2 2737 6643; fax: +886 2 2737 6644.
E-mail address: hml@ch.ntust.edu.tw (H.-M. Lin).

1385-8947/$ – see front matter © 2008 Published by Elsevier B.V.
doi:10.1016/j.cej.2007.12.008

In the earlier studies, Yeo et al. [14] investigated the preparation of micrometric particles of insulin by using supercritical carbon dioxide as anti-solvent. To further reduce the mean size of particulate protein, Chattopadhyay and Gupta [15] equipped a mass transfer enhancement unit with an SAS apparatus. Nano-metric particles were obtained from their experiments. Lysozyme, a small enzyme that can destroy the structural integrity of the cell walls of bacteria, is one of the most studied proteins in recent years. Several investigators [2,16–18] explored the effects of process parameters on the morphology and the size distribution of the particulates lysozyme prepared with supercritical fluid-assisted methods. However, it appears that no consistently conclusive results have been achieved up to date. Winters et al. [19] measured the biological activity (BA) of lysozyme particles precipitated under different operating conditions. After the SAS processing, the biological activities of the lysozyme particles were found to retain about 88–100% in comparing with those of the untreated lysozyme. Moshashaee et al. [20,21] reported that the BA of particulate lysozyme depended on precipitated conditions and the precipitated pressure was one of the major factors. As evidenced from their experimental results, the percentage of retained BA increased with increasing precipitation pressure and reached to 100% as pressures were sufficiently high.

Reverchon et al. [22,23] reported that sub-micrometric yttrium acetate (YAc) particles were generated when a homogenous supercritical phase was formed in the precipitator. Micrometric powders were produced as the operating conditions below the mixture critical point (MCP) of the mixtures, and balloon-like particles were obtained from precipitation in the superheated vapor phase region.

In the present study, ultra-fine particles of lysozyme were prepared with the SAS method. The aim of this work is to explore the role of phase behavior in dominating the morphology and the dimension of the resulting products. A series of precipitation experiments was conducted at various conditions of the process parameters, including the inside diameter of capillary tube in the coaxial injector, the precipitation temperature and pressure, and the lysozyme concentration in the feed stream. The dynamic compositions of mixtures in the precipitator during SAS process were calculated from a CSTR model and the precipitating conditions were mapped onto the vapor–liquid phase diagram of carbon dioxide + DMSO to interpret the correlation of morphology and particle size of particulate products with the phase behavior of the solvent + anti-solvent mixtures in the precipitator during the particle formation period.

2. Experimental section

2.1. Apparatus and procedure

The schematic diagram of the SAS apparatus (model: SAS 200, Thar Technologies Co., USA) is illustrated in Fig. 1. The detailed description of this apparatus and its operating procedure has been given elsewhere [24]. At the beginning stage, carbon dioxide was liquefied with a cooler (3) and continuously delivered into the precipitator (10) via the outer part of the coaxial injector (9) by a high pressure liquid pump (11, P1) to reach a desired pressure. Temperature of the precipitator was regulated to a pre-specified level by a heating jacket (8). As a steady-state was achieved, the solution of lysozyme dissolved in DMSO was charged by another high pressure pump (11, P2) at a given flow rate and injected into the precipitator through a coaxial injector (9). The injection system was composed of a 0.3175 cm (OD) stainless steel tube with an insert of 0.15875 cm (OD) PEEK capillary tube (Victrex, UK). During the precipitation stage, the flow rate of carbon dioxide was maintained at about 30 g/min (4) in each run. Upon the fine droplets of the lysozyme solution contacting with supercritical carbon dioxide in the precipitator, DMSO escaped from the liquid droplets to the vapor phase suddenly and thus lysozyme particles were formed due to supersaturation. The precipitation stage was completed within about 90–150 s. After that, carbon dioxide was continuously delivered to remove the residual solvent in the precipitator. This drying stage lasted for about 2–3 h. The precipitation vessel was then depressurized gradually to atmospheric pressure. Finally, the samples of resultant particles were taken from the precipitator for further characterization analysis.

2.2. Materials

Lysozyme (purity of 95%) made from chicken egg white (molecular weight about 14.3 kDa) was supplied by Sigma–Aldrich (USA). Fig. 2 shows the morphology of the lyophilized powders as received. DMSO (purity of 99.9%, spectrophotometric grade) was purchased from Arcos Organic (USA) and carbon dioxide (purity of 99.5+%) from Liu-Hsiang Gas Co. (Taiwan). These chemicals were used without further purification. Deionized pure water was prepared in our laboratory.

2.3. Characterization analysis

The morphology of particulate samples was observed with field emission scanning electron microscope (FESEM) (JSM-6500F JEOL, Japan). The sample particles were fixed on the specimen holder by the double-sided tape, and then sputter-coated with a thin film of platinum. The mean particle size and the PSD of the primary particles were determined with the aid of Sigma Scan Pro 5 software. At least 300 particles were counted from each FESEM image for mean particle size determination.

The thermal property of lysozyme samples was analyzed with DSC (Pyris 1, PerkinElmer, USA) from 313 K to 413 K. A sample of about 2 mg was sealed in an aluminum standard pan, and then heated at a fixed temperature increment of 10 K/min to obtain the thermal histogram.

The X-ray diffraction (XRD) patterns of the unprocessed lysozyme and the SAS processed lysozyme particles were obtained from WAXS (PSAXS-USH-WAXS-002, Osmic Inc., USA). The WAXS measurements were performed at room temperature and the samples were held in a vacuum chamber. The diffractograms were collected over a range of 2θ from 6.5° to 60° to analyze the crystallinity of the samples.

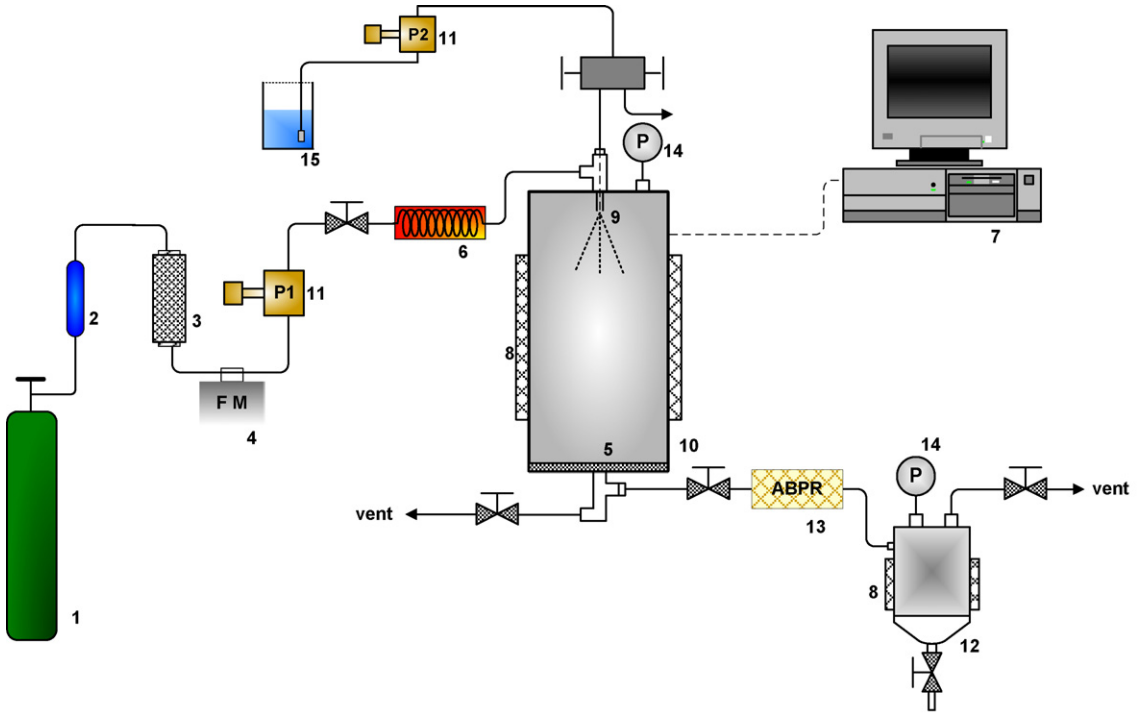

Fig. 1. Schematic diagram of the supercritical anti-solvent apparatus.

The PSD of particulate samples were also measured with DLS particle size analyzer (Model: ZEN3690, Malvern Instruments Ltd., UK). A standard sample (3060, Nanosphere^{TM} Size Standards, certified mean diameter = 60 ± 2.7 nm, Duke Scientific Co., USA) was used to calibrate the outputs of DLS. An appropriate amount of lysozyme particles was dispersed in deionized water, and the suspension solution was treated with ultrasonication (Model: D150H, Delta New Instrument Co., Taiwan) before analysis. The DLS measurements were conducted at 298 K and three replications were made for each particulate sample.

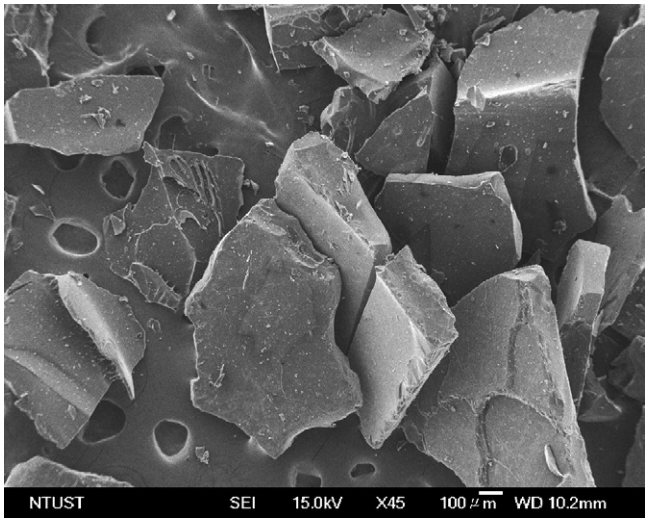

Fig. 2. FESEM image of received lyophilized lysozyme.

3. Results and discussion

The SAS apparatus, as mentioned above, was used in the present study to produce ultra-fine particles of lysozyme by using DMSO as a solvent and carbon dioxide as an anti-solvent. The precipitation conditions and the corresponding results were listed in Table 1. The influences of several process parameters on the morphology and the mean size of the particulate samples were investigated. These parameters included the inside diameter of capillary tube, the precipitation pressure (P) and temperature (T), and the lysozyme concentration (C). The experimental results are discussed as follows.

3.1. Phase diagram of solvent/anti-solvent mixtures

According to our previous studies on particle formation of metallocene-catalyzed cyclic olefin copolymer (mCOC) via the

Table 1
Experimental conditions and corresponding results

Runs #	T (K)	P (MPa)	C (wt%)	F (g/min)	Capillary size (μm)	Mean size of primary particles (nm)	Standard deviation (nm)	Figure number of FESEM	Product's morphology
1	308.2	15	0.7	5	508	91	13	Fig. 5(a)	Agglomerated nano-particles
2	308.2	7	0.7	5	254	189	37	Fig. 6(a)	Agglomerated spheres
3	308.2	8.5	0.7	5	254	98	17	Fig. 6(b)	Irregular nano-particles
4	308.2	10	0.7	5	254	99	16	–	Irregular nano-particles
5	308.2	12	0.7	5	254	101	15	Fig. 6(c)	Irregular nano-particles
6	308.2	15	0.7	5	254	74	9	Fig. 5(b)	Uniform nano-particles
7	308.2	20	0.7	5	254	70	10	Fig. 6(d)	Uniform nano-particles
8	318.2	10	0.7	5	254	–	–	Fig. 7(a) and (b)	Various morphologies
9	328.2	10	0.7	5	254	–	–	Fig. 8(a)	Expanded microparticles
10	338.2	10	0.7	5	254	207	40	Fig. 8(b)	Agglomerated spheres
11	308.2	15	0.35	5	254	67	8	–	Uniform nano-particles
12	308.2	15	1.5	5	254	70	9	–	Uniform nano-particles
13	308.2	15	3.0	5	254	73	12	–	Uniform nano-particles

SAS process [24], the vapor–liquid equilibrium (VLE) phase diagram of solvent + anti-solvent binary system can provide us useful information to control the morphology and the mean size of the particulate products by manipulating the precipitation conditions. Because the solubility of proteins in carbon dioxide was generally rather minute [25] and the concentrations of lysozyme in the injected solution were also very dilute, the influence of the presence of lysozyme on the VLE phase boundaries of the ternary system would be insignificant. Among several others, the vapor–liquid phase boundaries of carbon dioxide + DMSO binary system have been measured in our laboratory [26] with a visual and volume-variable phase equilibrium analyzer at temperatures from 318.15 K to 348.15 K and pressure up to 18 MPa, including near critical regions. The phase diagram is illustrated graphically in Fig. 3, where the phase envelope of 309.41 K was determined experimentally by Gonzalez et al. [27]. According to this phase diagram, the critical pressures were estimated to be about 8 MPa at 308.2 K, 10 MPa at 318.2 K, 12.7 MPa at 328.2 K, 15.2 MPa at 338.2 K, and 17.7 MPa at 348.2 K, respectively.

Schmitt et al. [28] developed a simple continuous stirred tank reactor (CSTR) with two independent inlet and one outlet stream to describe the operation of SAS process. We employed their mathematical model in this work to estimate the compositions of mixtures in the precipitator varying with injection time during the precipitating stage. The derivation of the modeling has been given elsewhere [28,29]. The minimum mole fraction of carbon dioxide in the precipitator occurred at the end of injec-

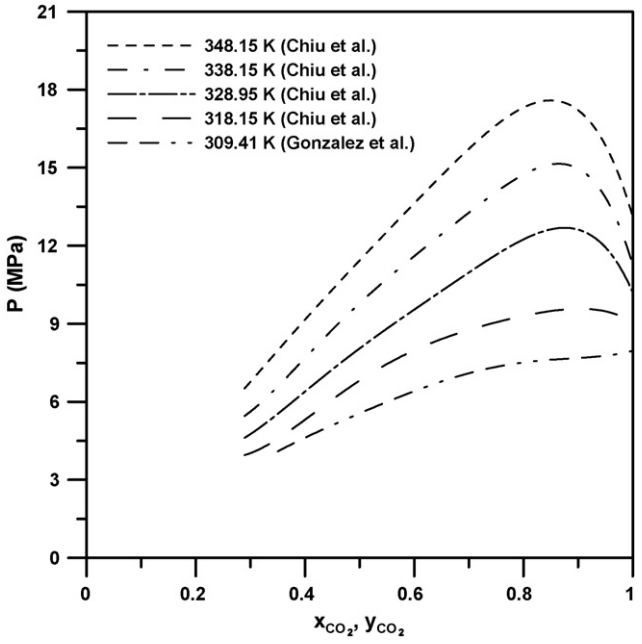

Fig. 3. VLE phase diagram of carbon dioxide + DMSO system.

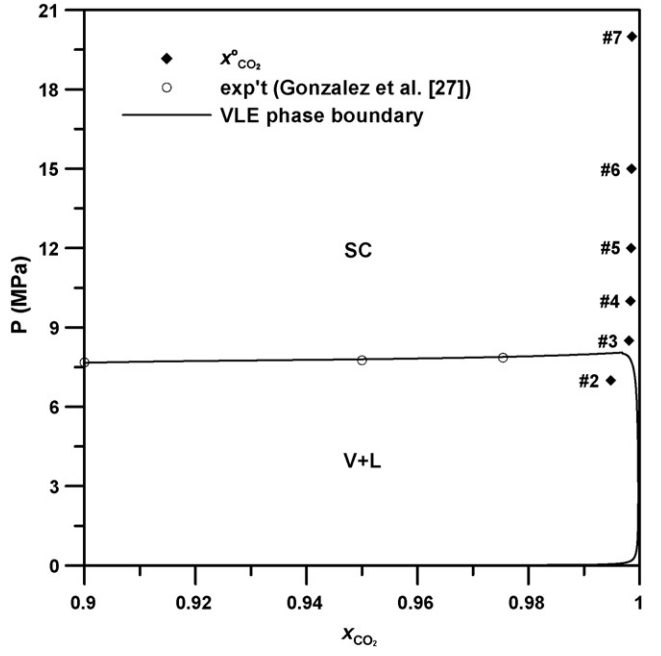

Fig. 4. VLE phase boundary and the estimated concentrations of carbon dioxide in precipitator at the end of injection of protein solution for the experimental runs at 308.2 K.

tion of protein solution ($x^0_{CO_2}$). As a representative illustration, the values of $x^0_{CO_2}$ were marked in Fig. 4 for several precipitation runs which were conducted at 308.2 K. In this graph, the solid curve refers to the VLE phase boundaries of DMSO + CO_2, SC means supercritical region, and V + L represents vapor–liquid coexistence region. The particles were formed in the supercritical region when the point of $x^0_{CO_2}$ was located well above the mixture critical point (MCP). Runs #1, #3–7, #11–13 were all made in the homogeneous supercritical phase region. While run #8 was operated near the critical region, the dynamic concentration loci of runs #2 and #10 were starting from superheated vapor region, passing through the phase boundary, and ending in the vapor–liquid coexistence region at the end of solution injection period. Run #9 is a special case in this series of experiments whose precipitation pressure, 10 MPa, is below the corresponding critical pressure (12.7 MPa at 328.2 K). However, its $x^0_{CO_2}$ value, about 0.9965, is still greater than the corresponding dew-point composition, about 0.99. This run should be operated in the superheated vapor region through the precipitation period.

3.2. Effect of the inside diameter of capillary tube

Two different sizes of capillary tube (508 μm and 254 μm) were tested at the same operating conditions (run #1 and run #6 as listed in Table 1). These two runs were conducted at pressure (15 MPa) well above the MCP (about 8 MPa at 308.2 K), in which the mixtures in the precipitator formed a homogenous supercritical state according to the vapor–liquid equilibrium phase diagram (Fig. 3). Additionally, the concentration of lysozyme in DMSO was fixed at 0.7 wt% and the injection rate of lysozyme solution (F) was maintained at 5 g/min. The particulate samples obtained from runs #1 and #6 are compared in Fig. 5, where the FESEM images were taken at the same magnification. While larger particles (mean size of 91 nm for the primary particles) with serious aggregation were obtained by using 508 μm capillary tube (run #1, Fig. 5(a)), smaller spherical primary nano-particles (mean size of 74 nm) with less agglomeration were produced by using 254 μm capillary tube (run #6, Fig. 5(b)). It was suggested that the smaller inside diameters of capillary tube could effectively atomize the solution to form the finer droplets [30,31]. This trend is consistent with the observations of the preparation of pigment particles by Wu et al. [32]. Therefore, the capillary tube with inside diameter of 254 μm was adopted in the rest of the precipitation experiments.

3.3. Effect of the precipitation pressure

The influence of the precipitation pressure on the morphology and the mean size of resulting particles were studied in a range of 7–20 MPa. In the series of runs (from runs #2 to #7), the temperature was maintained at 308.2 K and all the other operating parameters were also kept at the same levels. Fig. 6 shows the FESEM images for the particulate samples taken from different precipitation pressures. Fig. 6(a) depicts that agglomeration of submicron primary particles (mean size of 189 nm) with broad distribution was obtained as the precipitation was implemented in the vapor–liquid coexistence region of carbon dioxide + DMSO (at 7 MPa and 308.2 K). When the precipitation pressures were in the range of 8.5–12 MPa, slightly higher than the critical pressure of carbon dioxide + DMSO at 308.2 K, fused irregular nano-particles were produced as illustrated in Fig. 6(b) and (c). As shown in Figs. 5(b) and 6(d), spherical networked nano-particles were obtained when the precipitation pressures were higher than 15 MPa. Similar to the particle formation of α-chymotrypsin [33,34], the mean sizes of particulate samples became insensitive to pressure while the operating pressures were sufficiently higher than the corresponding critical pressure.

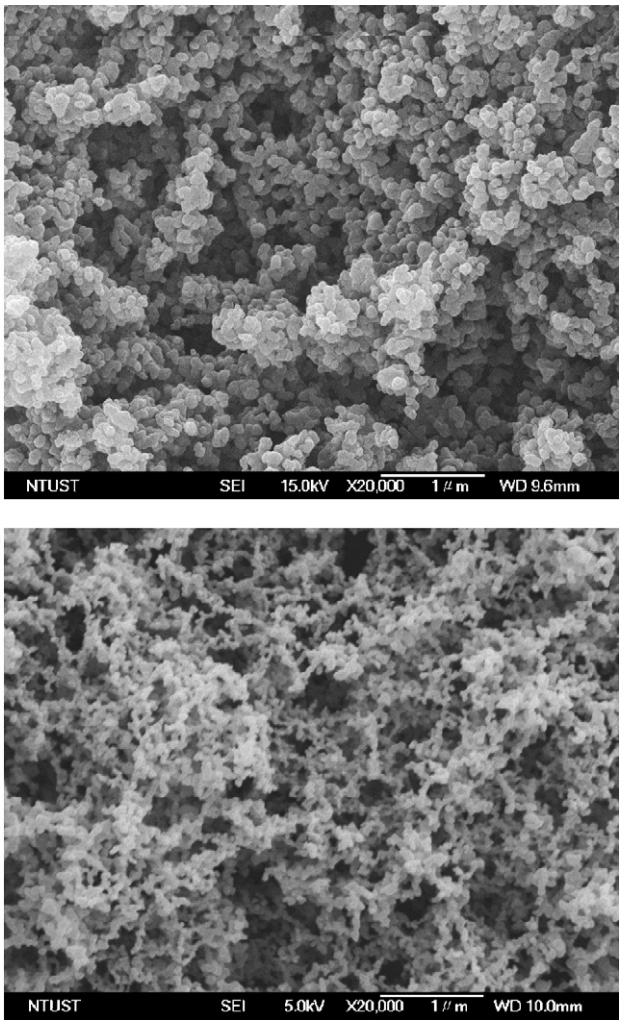

Fig. 5. FESEM images of lysozyme particles produced from the SAS process at P = 15 MPa, T = 308.2 K, C = 0.7 wt%, F = 5 g/min by using different inside diameters of capillary tube: (a) 508 μm and (b) 254 μm.

3.4. Effect of the precipitation temperature

The effect of the precipitation temperature on the resultant particles was observed at temperatures ranging from 308.2 K

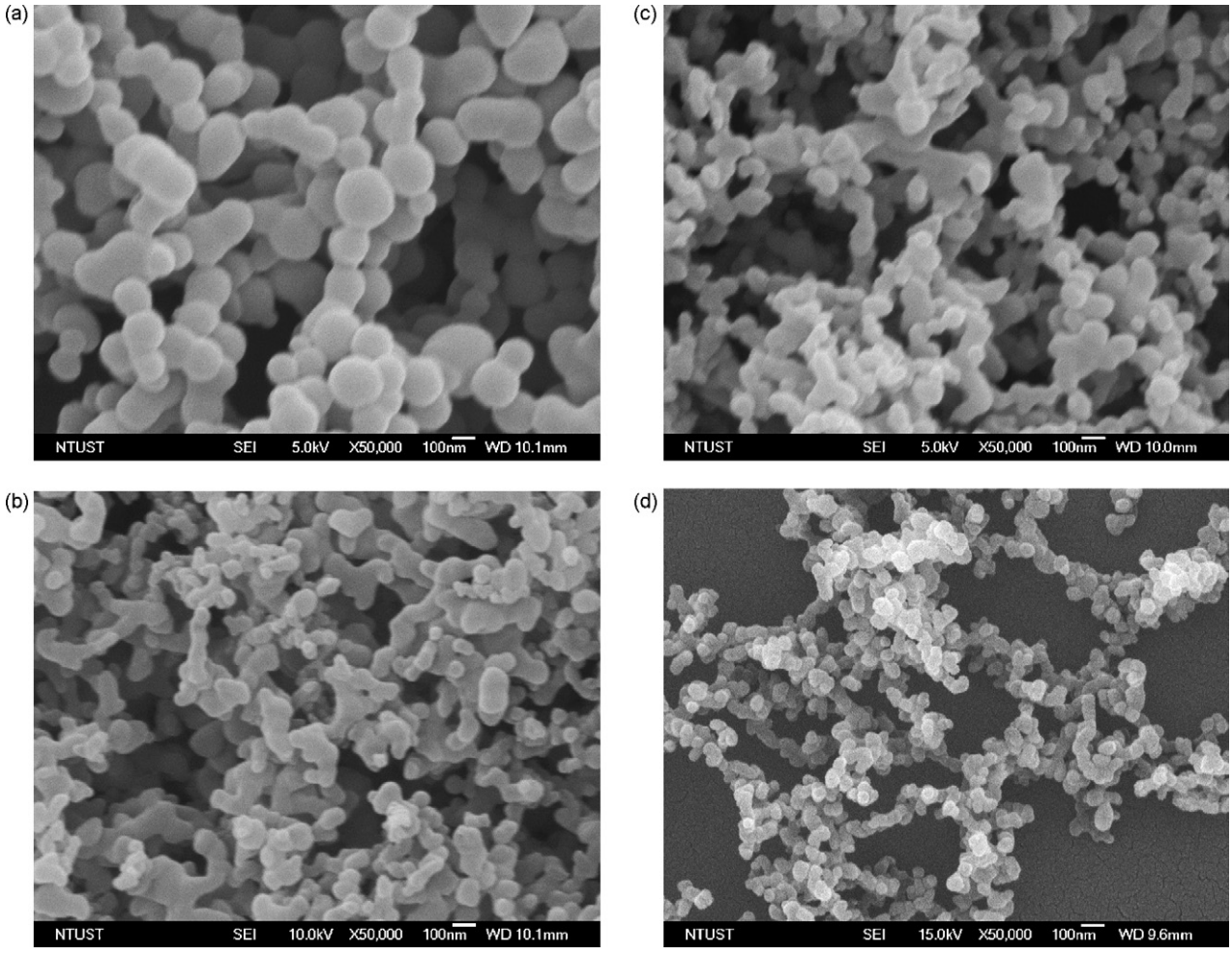

Fig. 6. FESEM images of lysozyme particles produced from the SAS process at $T = 308.2$ K, $C = 0.7$ wt%, $F = 5$ g/min, and precipitation pressures $P =$ (a) 7 MPa; (b) 8.5 MPa; (c) 12 MPa and (d) 20 MPa.

to 338.2 K (runs #4 and #8–10). In this series of runs, the rest of experimental conditions were fixed at $P = 10$ MPa, $C = 0.7$ wt% and $F = 5$ g/min, respectively. In the case of the precipitation temperature at 308.2 K (run #4), the particulate products are fused nano-particles, whose morphology is similar to that shown in Fig. 6(b). As the precipitation temperature was increased up to 318.2 K (run #8), various types of morphologies were exhibited simultaneously as presented in Fig. 7(a) which included micro-scale porous clusters, and irregular submicron and micron-metric aggregated particles. Fig. 7(b), an enlarged magnification of the FESEM image, shows that those micron-metric porous clusters are composed of a large amount of fine primary particles. According to the VLE phase diagram of carbon dioxide + DMSO (Fig. 3), the critical pressure is around 10 MPa at 318.2 K which is in the vicinity of run #8. Small fluctuation of the operating conditions during the precipitation may change the phase states of mixtures in the precipitator, leading to produce various types of morphologies of resultant particles. When the precipitation conditions were controlled at 328.2 K and 10 MPa (run #9), the mixtures in the precipitator are in the superheated vapor region. In this phase region, expanded microparticles (ranging from 5 μm to 20 μm) were formed as shown in Fig. 8(a). When the precipitation temperature was as high as 338.2 K (run #10), the mixtures in the precipitator were in vapor–liquid coexistence region. In this two-phase region, sub-micrometric lysozyme particles (about 200 nm) seriously aggregated to form a dense cake on the surface of the filter as illustrated in Fig. 8(b). Its morphology is similar to that observed from run #2 (Fig. 6(a)). According to the results of above experiments, it is found that the phase behavior of mixtures in the precipitator, during the precipitation stage, is one of the crucial factors to govern the product's morphology and PSD, in agreement with the observations by Reverchon et al. [22] and Wu et al. [29].

3.5. Effect of the lysozyme concentration

Another series of precipitation experiments (runs #6 and #11–13) was also made under different concentrations of lysozyme in DMSO, ranging from 0.35 wt% to 3 wt%. All these runs were operated at 15 MPa and 308.2 K (corresponding to the supercritical state of carbon dioxide + DMSO system), while

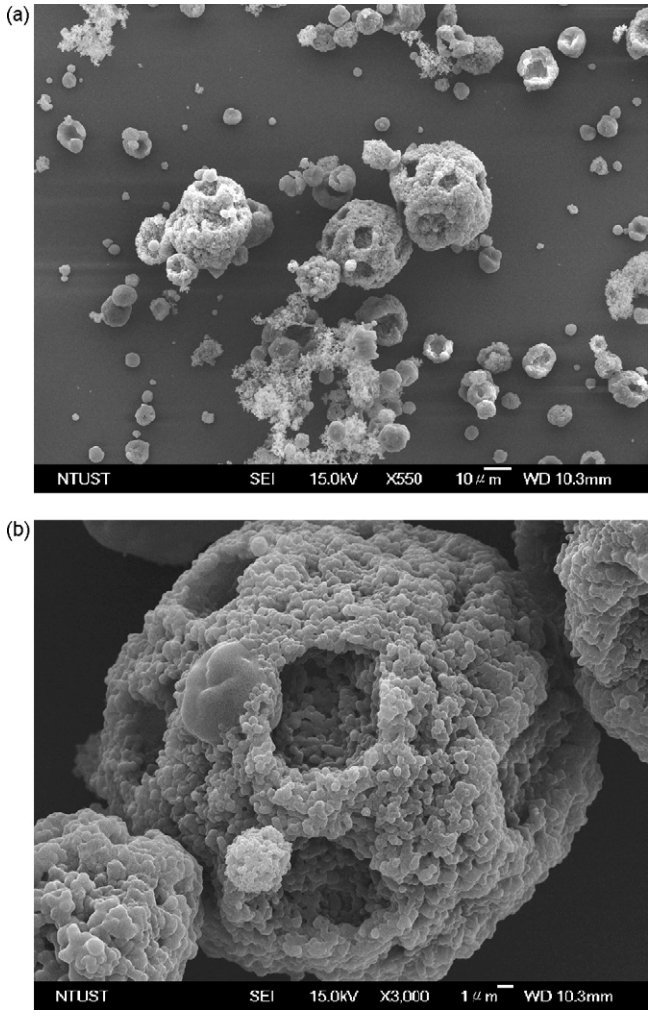

Fig. 7. FESEM images of lysozyme particles produced from the SAS process at $P = 10$ MPa, $T = 318.2$ K, $C = 0.7$ wt%, $F = 5$ g/min with the magnifications: (a) 550× and (b) 3000×.

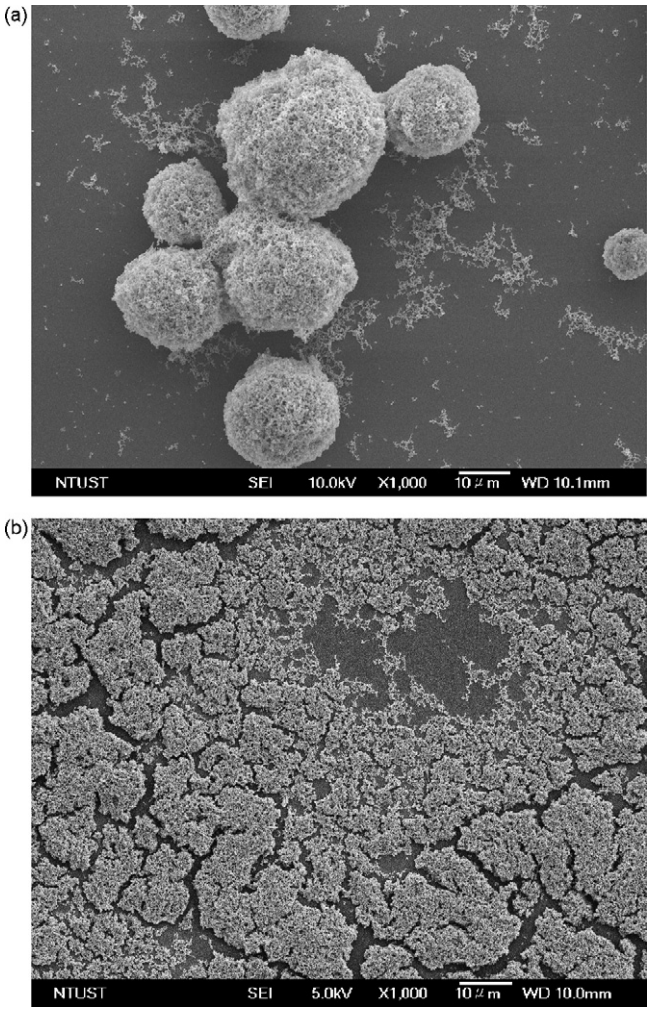

Fig. 8. FESEM images of lysozyme particles produced from the SAS process at $P = 10$ MPa, $C = 0.7$ wt% and $F = 5$ g/min at different precipitation temperatures: (a) 328.2 K and (b) 338.2 K.

the injection rate of lysozyme solutions was manipulated at 5 g/min. Fig. 9 shows the mean size and the standard deviation of the resultant primary particles varying with lysozyme concentration. It indicates that the mean size of the particulate products is relatively insensitive to lysozyme concentration, when the particles were prepared in the supercritical region. This finding is consistent with the observations of the particles formation for insulin by Yeo et al. [14]. Bustami et al. [16] reported that the smaller mean sizes of resultant particles with less degree of agglomeration were obtained from the higher concentrations of protein solutions, whereas our previous study on α-chymotrypsin indicated that the mean size of particle samples increased with increasing the concentration of the protein in DMSO [33,34]. The discrepant trends observed from various protein-containing systems may be attributable to the different sensitivities on the changes of phase transition boundaries for the mixtures of carbon dioxide + DMSO in the presence of the third component. Reverchon et al. [22] investigated the phase behavior of CO_2 + DMSO + YAc ternary system with a visual cell during the precipitation stage. They

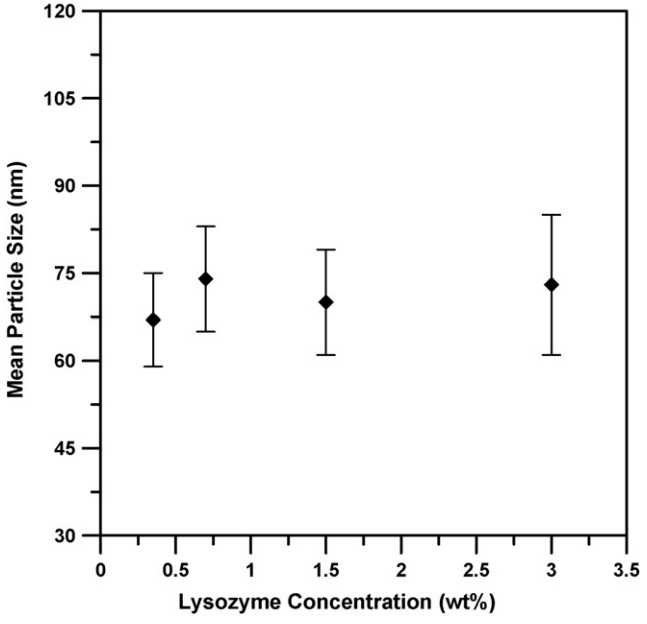

Fig. 9. Mean particle size varying with lysozyme concentrations at $P = 15$ MPa, $T = 308.2$ K and $F = 5$ g/min.

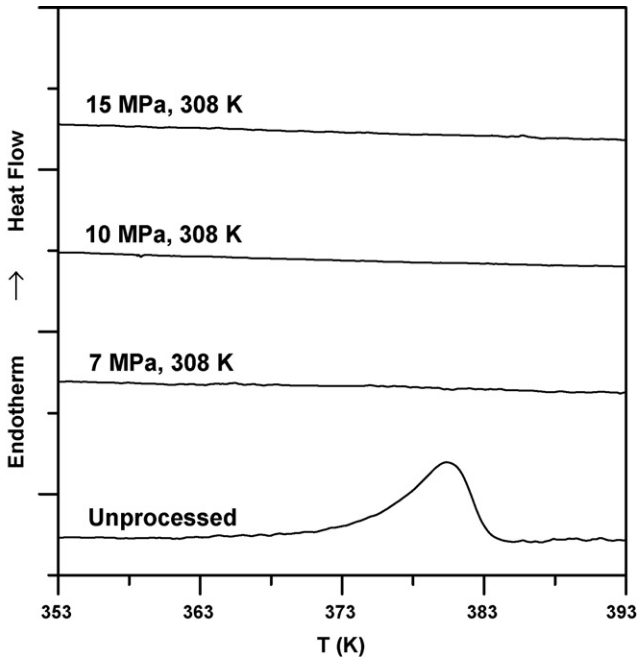

Fig. 10. Thermograms of unprocessed lysozyme and samples produced from the SAS process at $T = 308.2$ K, $C = 0.7$ wt% and $F = 5$ g/min under precipitation pressures from 7 MPa to 15 MPa.

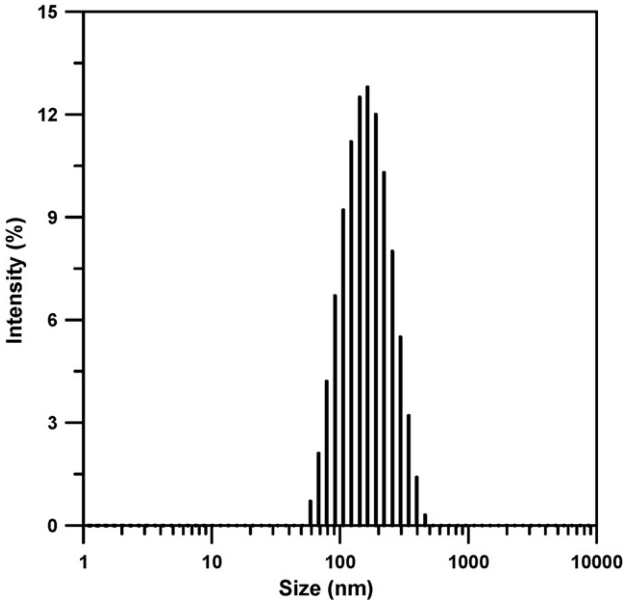

Fig. 12. Particle size distribution measured with DLS for the lysozyme particles precipitated from the SAS process at $P = 8.5$ MPa, $T = 308.2$ K, $C = 0.7$ wt% and $F = 5$ g/min.

found that the influence of the presence of dilute solute concentration on mixture's phase boundaries was insignificant. However, the vapor–liquid phase transition pressures of the ternary system may increase with an increase of solute concentrations if the concentrations are sufficiently high. Since similar morphology and PSD of particulate products were found in the present study under four different lysozyme concentrations (0.35–3 wt%), it could be implied that the critical pressure of the ternary system at 308.2 K is still well below 15 MPa even the lysozyme concentration as high as 3 wt%, i.e., all these four runs were conducted in the same phase region (i.e., at supercritical states).

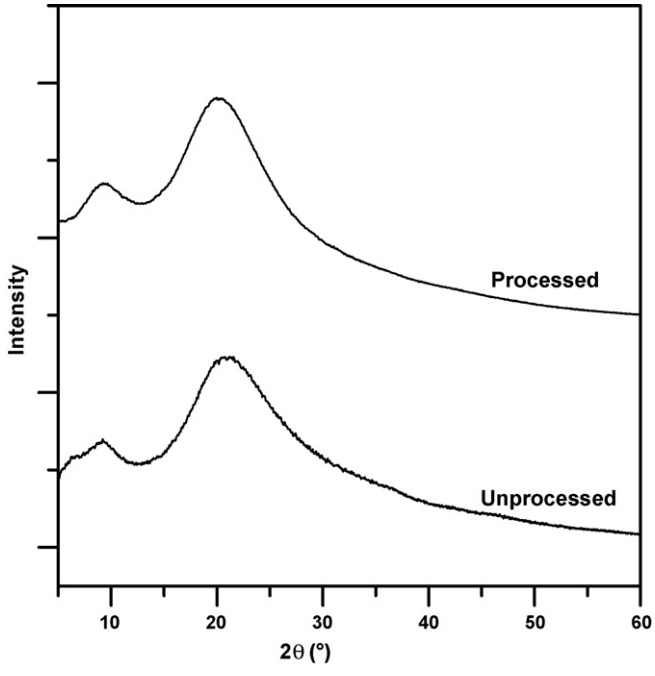

Fig. 11. XRD patterns of unprocessed lysozyme and samples precipitated from the SAS process.

3.6. Physicochemical characterization

The thermal properties were analyzed by DSC for the raw lysozyme and the particulate samples after SAS processing. As seen form Fig. 10, the DSC thermograms show an endothermic dehydration peak at about 380 K for the unprocessed lysozyme. However, the dehydration peak disappears from those of the particulate samples, which were prepared under different precipitation conditions.

The XRD diffractograms are shown in Fig. 11, revealing that both the untreated lysozyme and the processed samples are completely amorphous. The XRD patterns, both the peak location and the intensity, are similar to those from the particle preparation from lysozyme aqueous solutions by using supercritical fluid drying [35].

The PSD of particulate samples dispersed in water were also measured by DLS. Fig. 12 depicts the PSD of a representative sample prepared from run #3 (at 8.5 MPa and 308.2 K). The mean size of the sample is 132 nm with the polydispersity index (PDI) of 0.257. This result is generally consistent with the mean size of primary particles determined from the FESEM image, indicating that the agglomerated primary particles can be well separated and dispersed in water by ultrasonication.

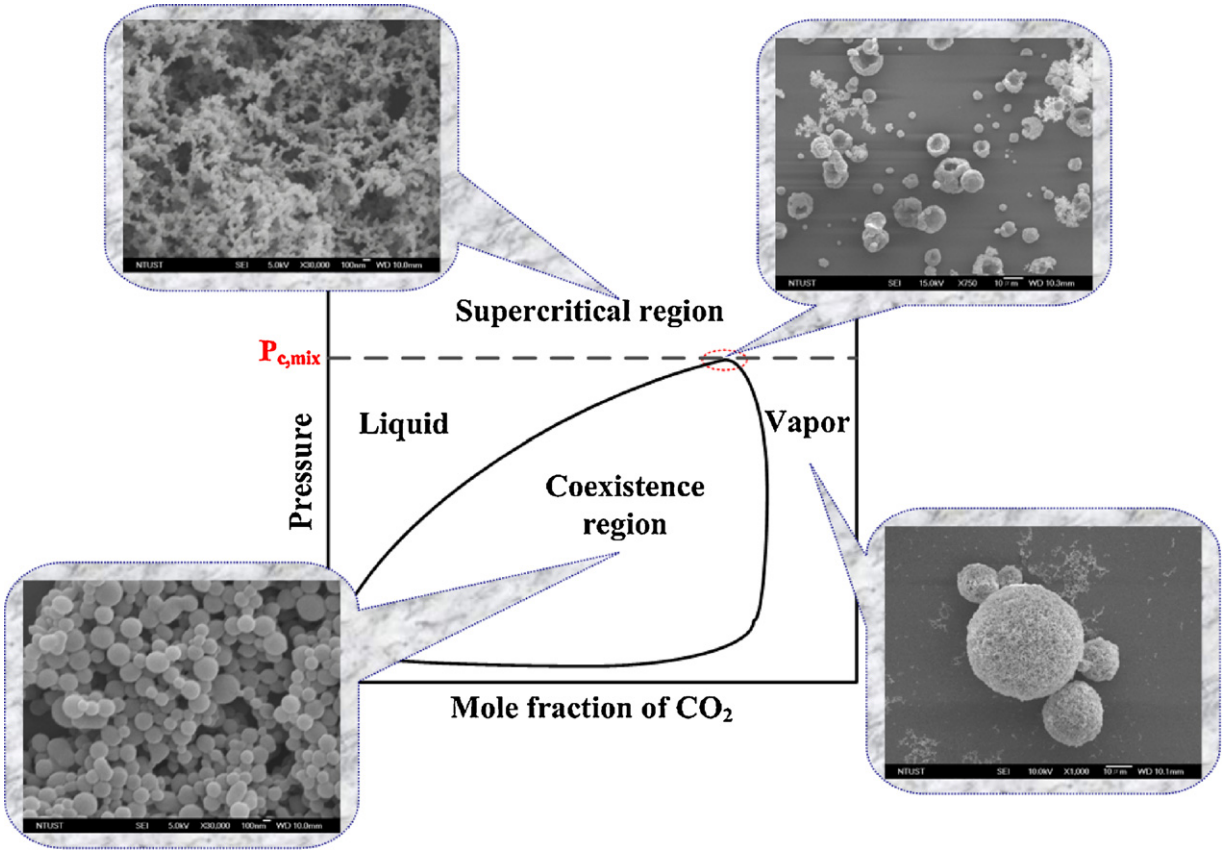

Fig. 13. FESEM images of lysozyme particles prepared in different phase regions.

4. Conclusions

A model protein lysozyme was successfully micronized to ultra-fine particles via the SAS process with DMSO as a solvent and carbon dioxide as an anti-solvent. The effects of the size of capillary tube, the precipitation pressure and temperature, and the lysozyme concentration, on the morphology and the mean size of particulate samples have been investigated. It was found that using smaller size of injection capillary tube was favorable to reduce the mean size of the resultant particles. As also evidenced from the experimental results, the phase behavior of mixtures in the precipitator during the precipitation stage should be one of the crucial factors to control the morphology and the PSD of the particulate products in the SAS process. Fig. 13 illustrates the FESEM images of the particulate samples obtained from different phase regions. As seen from this graph, uniform networked nano-particles were produced as the precipitation was implemented in the supercritical region. Various types of morphologies of the resulting products were exhibited when the precipitation was made around the near critical region. Spherical micron-metric clusters were formed in the superheated vapor region, while sub-micrometric particles were aggregated as a dense cake on the surface of the filter when the precipitation conditions were manipulated in the vapor–liquid coexistence region. While the DSC thermograms indicated that water content in the original lysozyme was removed through the SAS process, the XRD patterns revealed that both the original lysozyme and the samples after SAS processing were completely amorphous. Additionally, the mean size of particulate sample dispersed in pure water measured with DLS was qualitatively consistent with that of the primary particles determined from FESEM image. It means that the aggregated primary nano-particles prepared from the SAS process can be disintegrated and dispersed in water by ultrasonication.

References

[1] M.C. Manning, K. Patel, R.T. Borchardt, Stability of protein pharmaceuticals, Pharm. Res. 6 (1989) 903–918.
[2] S.P. Sellers, G.S. Clark, R.E. Sievers, J.F. Carpenter, Dry powders of stable proteins formulations from aqueous solutions prepared using supercritical CO_2-assisted aerosolization, J. Pharm. Sci. 90 (2001) 785–797.
[3] D.W. Matson, J.L. Fulton, R.C. Peterson, R.D. Smith, Rapid expansion of supercritical fluid solutions: solute formation of powders, thin films, and fibers, Ind. Eng. Chem. Res. 26 (1987) 2298–2306.
[4] M. Rodrigues, N. Peiriço, H. Matos, E. Gomes de Azevedo, M.R. Lobato, A.J. Almeida, Microcomposites theophylline/hydrogenated palm oil from a PGSS process for controlled drug delivery systems, J. Supercrit. Fluids 29 (2004) 175–184.
[5] D.J. Dixon, K.P. Johnston, R.A. Bodmeier, Polymeric materials formed by precipitation with a compressed fluid anti-solvent, AIChE J. 39 (1993) 127–139.
[6] E. Reverchon, Supercritical-assisted atomization to produce micro- and/or nanoparticles of controlled size and distribution, Ind. Eng. Chem. Res. 41 (2002) 2405–2411.
[7] R.E. Sievers, S.P. Sellers, J.F. Carpenter, Supercritical fluid-assisted nebulization and bubble drying, World International Property Organization WO0075281 (2000).

[8] J. Jung, M. Perrut, Particle design using supercritical fluids: literature and patent survey, J. Supercrit. Fluids 20 (2001) 179–219.
[9] C. Vemavarapu, M.J. Mollan, M. Lodaya, T.E. Needham, Design and process aspects of laboratory scale SCF particle formation systems, Int. J. Pharm. 292 (2005) 1–16.
[10] E. Reverchon, R. Adami, Nanomaterials and supercritical fluids, J. Supercrit. Fluids 37 (2006) 1–22.
[11] J.S. Patton, P. Trinchero, R.M. Platz, Bioavailability of pulmonary delivered peptides and proteins: α-interferon, calcitonins and parathyroid hormones, J. Control. Release 28 (1994) 79–85.
[12] A. Adjei, J. Garren, Pulmonary delivery of peptide drugs: effects of particles size on bioavailability of leuprolide acetate in healthy human male volunteers, Pharm. Res. 7 (1990) 565–569.
[13] M.C. Lai, E.M. Topp, Solid-state chemical stability of proteins and peptides, J. Pharm. Sci. 88 (1999) 489–500.
[14] S.D. Yeo, G.B. Lim, P.G. Debenedetti, H. Bernstein, Formation of microparticulate protein powders using a supercritical fluid antisolvent, Biotechnol. Bioeng. 41 (1993) 341–346.
[15] P. Chattopadhyay, R.B. Gupta, Protein nanoparticles formation by supercritical antisolvent with enhanced mass transfer, AIChE J. 48 (2002) 235–244.
[16] R.T. Bustami, H.K. Chan, F. Dehghani, N.R. Foster, Generation of microparticles of proteins for aerosol delivery using high pressure modified carbon dioxide, Pharm. Res. 17 (2000) 1360–1366.
[17] G. Muhrer, M. Mazzotti, Precipitation of lysozyme nanoparticles from dimethyl sulfoxide using carbon dioxide as antisolvent, Biotechnol. Prog. 19 (2003) 549–556.
[18] N. Jovanović, A. Bouchard, G.W. Hofland, G.J. Witkamp, D.J.A. Crommelin, W. Jiskoot, Stabilization of proteins in dry powder formulations using supercritical fluid technology, Pharm. Res. 21 (2004) 1955–1969.
[19] M.A. Winters, B.L. Knutson, P.G. Debenedetti, H.G. Sparks, T.M. Przybycien, C.L. Stevenson, S.J. Prestrelski, Precipitation of proteins in supercritical carbon dioxide, J. Pharm. Sci. 85 (1996) 586–594.
[20] S. Moshashaee, M. Bisrat, R.T. Forbes, H. Nyqvist, P. York, Supercritical fluid processing of proteins. I. Lysozyme precipitation from organic solution, Eur. J. Pharm. Sci. 11 (2000) 239–245.
[21] S. Moshashaee, M. Bisrat, R.T. Forbes, E.A. Quinn, H. Nyqvist, P. York, Supercritical fluid processing of proteins: lysozyme precipitation from aqueous solution, J. Pharm. Pharmacol. 55 (2003) 185–192.
[22] E. Reverchon, G. Caputo, I. De Marco, Role of phase behavior and atomization in the supercritical antisolvent precipitation, Ind. Eng. Chem. Res. 42 (2003) 6406–6414.
[23] E. Reverchon, Micro and nano particles produced by supercritical fluids assisted techniques: present status and future developments, Chem. Eng. Trans. 2 (2002) 1–10.
[24] S.C. Chang, M.J. Lee, H.M. Lin, Nanoparticles formation for metallocene catalyzed cyclic olefin copolymer via a continuous supercritical anti-solvent process, J. Supercrit. Fluids 40 (2007) 420–432.
[25] P.M. Gallagher, M.P. Coffey, V.J. Krukonis, N. Klasutis, Gas antisolvent recrystallization: new process to recrystallize compounds insoluble in supercritical fluids, ACS Symp. Ser. 406 (1989) 334–354.
[26] H.Y. Chiu, R.F. Jung, M.J. Lee, H.M. Lin, Vapor–liquid phase equilibrium behavior of mixtures containing supercritical carbon dioxide near critical region, J. Supercrit. Fluids 44 (2008) 273–278.
[27] A.V. Gonzalez, R. Tufeu, P. Subra, High-pressure vapor–liquid equilibrium for binary systems carbon dioxide + dimethyl sulfoxide and carbon dioxide + dichloromethane, J. Chem. Eng. Data 47 (2002) 492–495.
[28] W.J. Schmitt, M.C. Salada, G.G. Shook, S.M. Speaker III, Finely-divided powders by carrier solution injection into a near or supercritical fluid, AIChE J. 41 (1995) 2476–2486.
[29] H.T. Wu, M.J. Lee, H.M. Lin, Ultra-fine particles formation of C.I. pigment green 36 in different phase regions via a supercritical anti-solvent process, Dyes Pigments 75 (2007) 328–334.
[30] S.S. Dukhin, C. Zhu, R. Dave, R. Pfeffer, J.J. Luo, F. Chavez, Y. Shen, Dynamic interfacial tension near critical point of a solvent–antisolvent mixture and laminar jet stabilization, Colloids Surf. A 229 (2003) 181–199.
[31] W.Z. He, Q.L. Suo, Z.H. Jiang, S.A.H.L. Hong, Precipitation of ephedrine by SEDS process using a specially design prefilming atomizer, J. Supercrit. Fluids 31 (2004) 101–110.
[32] H.T. Wu, M.J. Lee, H.M. Lin, Nano-particles formation for pigment red 177 via a continuous supercritical anti-solvent process, J. Supercrit. Fluids 33 (2005) 173–182.
[33] S.C. Chang, M.J. Lee, H.M. Lin, The influence of phase behavior on the morphology of protein α-chymotrypsin prepared via a supercritical antisolvent process, in: Proceedings of the Eighth International Symposium on Supercritical Fluids, Kyoto, Japan, November 5–8, 2006.
[34] S.C. Chang, M.J. Lee, H.M. Lin, The influence of phase behavior on the morphology of protein α-chymotrypsin prepared via a supercritical antisolvent process, J. Supercrit. Fluids 44 (2008) 219–229.
[35] A. Bouchard, N. Jovanović, W. Jiskoot, E. Mendes, G.J. Witkamp, J.A. Daan, J.A. Crommelin, G.W. Hofland, Lysozyme particle formation during supercritical fluid drying: particle morphology and molecular integrity, J. Supercrit. Fluids 40 (2007) 293–307.